JOSEPHSON TRAVELING-WAVE ANTENNAS

V. V. Kurin,* **N. K. Vdovicheva, and**
I. A. Shereshevskii
UDC 537.9

We propose a new approach to the problem of obtaining coherent radiation from systems with a great number of Josephson junctions, which is based on the concept of traveling-wave antennas. The traveling wave in a line ensures identity of the electrodynamic conditions, under which the junctions operate, whereas the energy leakage to radiation in the lateral direction prevents saturation of the nonlinearity of the individual junctions having a small dynamic range. Simple analytical models, which demonstrate feasibility of the traveling-wave regime, are considered. A code for direct numerical simulation of Josephson microchips including microantennas, lumped elements, and power supply circuits have been developed. Using the direct numerical simulation, a version of the Josephson antenna, which is similar to the simplest single-wire antenna, is studied and the possibility to realize the traveling-wave regime is demonstrated.

1. INTRODUCTION

The idea of using the Josephson effect for generation of high-frequency electromagnetc radiation has attracted attention of scientists since the time of the discovery of this effect in 1962 [1]. When the voltage V is applied across the Josephson junction, which is a tunnel transition between superconductors, the junction generates an ac supercurrent with the frequency ω determined by the so-called Josephson relation $\hbar\omega = 2eV$, where $\hbar$ is Planck's constant and e is the elementary charge. A frequency of 0.486 THz corresponds to a voltage of 1 mV. By varying the voltage, one can vary the oscillation frequency smoothly up to the limiting frequency determined by the energy gap of the superconducting material, which the Josephson junction is made of. For niobium-based junctions, the limiting frequency is about 700 GHz, for those made of NbN, about 1.3 THz, and for internal Josephson junctions in layered high-temperature BiSrCaCuO superconductors, it is about 10 THz. Thus, the Josephson junction is a small-size, tunable source of terahertz waves, which is of utmost importance for possible applications in spectroscopy, atmosphere monitoring, and radio imaging.

However, the radiated power of an individual Josephson junction is very low due both to the small value of the ac component of the supercurrent, which is about 0.1 mA/μm^2, and a great mismatch between the junction impedance and the free-space impedance being $Z_0 = 120\pi$ Ω. An evident way to increase the radiated power and achieve good matching is related to the use of one- or two-dimensional arrays of lumped Josephson junctions and ensurance of the coherence of contributions from individual junctions. The second way is related to the use of large-size distributed Josephson junctions. Surely, both methods can be used in combination. A certain success has been achieved in this context, namely, generation in the frequency range 0.1–0.5 THz with a power of up to 1 μW inside the chip, which is, in principle, sufficient for the applications, is described in [2–5]. The most successful development was that of oscillator based

---

* kurin@ipmras.ru

on the motion of Josephson vortices in the distributed Josephson junctions. Currently, they find practical application as local oscillators for pumping of superconducting mixers [6]. A brilliant result reviving the interest in Josephson oscillators, which had burned out in some degree by the beginning of the XXIst century, was the discovery of microwave radiation in the terahertz range from mesostructures containing about a thousand of Josephson junctions based on a high-temperature BiSrCCuO superconductor with the internal Josephson effect [7]. The characteristics and mechanism of this radiation are intensely studied at present, and the state-of-the-art is described in review work [8]. Josephson oscillators based on planar arrays of small-size low-temperature junctions are also actively developed. Recently, the possibility of using such sources in practice as local oscillators of quasioptical receivers has been demonstrated in [9].

Despite significant progress, the field of applications of Josephson oscillators is still very narrow. In order to win a competition with semiconductor devices, such as terahertz quantum cascade lasers, the power of such oscillators should be increased significantly, up to, e.g., the level of several milliwatts. This requires making up systems which contain about 10^4–10^5 Josephson junctions. At a current integration level, such a microchip will have a dimension of about 1 cm, which corresponds to approximately 30 wavelengths λ of the terahertz range, for which $\lambda \approx 300~\mu$m. For such dimensions, the dynamics of the Josephson systems is influenced significantly by the effects of delay and radiation to free space. From the engineering viewpoint, the Josephson lines are usually planar structures, whereas the Josephson junctions, power circuits, and electrodynamic environment are located on the surface of a dielectric substrate. They can be single-wire, or multi-wire, strip, slot, or coplanar lines with built-in Josephson junctions.

In this work, we consider such large-size Josephson systems and present their theoretical description and computer simulation. We demonstrate that in some classes of such systems, traveling-wave regimes are possible, under which all Josephson junctions are under identical electrodynamic conditions and make coherent contributions to the radiation field. Such systems, which will be called active Josephson traveling-wave antennas, are scalable, i.e., in the case of optimal matching, the intensity of their radiation increases in proportion to the size of the system or the number of the Josephson junctions. An important component, which ensures coherence of the contributions made by a great number of junctions, is the lateral energy leakage from the transmission line (vertical radiation output), which prevents saturation of the nonlinearity of individual junctions with narrow dynamic ranges. Such systems can be used as a basis for Josephson oscillators producing power levels sufficient for practical applications. In this work, we develop the theory of open Josephson traveling-wave lines and find the conditions for existence and stability of such regimes. To study the nonlinear dynamics of active Josephson antennas, a numerical simulation code has been developed, which is based on the Finite Difference Time Domain (FDTD) method and a self-consistent solution of the nonlinear equations which describe the Josephson junctions. The results of simulation of some variants of Josephson traveling-wave antennas are presented.

The paper is organized as follows. First, we consider a simple model of the Josephson linear antenna, derive the basic equations describing its nonlinear dynamics, find their solutions in the form of traveling waves, and study their stability. Then we describe the scheme of numerical simulation of the dynamics of the Josephson antennas and present the results of simulation for a simple model which is the Josephson analog of the Beverage antenna [10]. Radiation patterns of these antennas are presented, which confirm the realization of the traveling-wave regime and a sufficiently high efficiency of the radiation.

2. BASIC EQUATIONS

As an example, consider a one-dimensional chain of junctions connected in series in the common power circuit and placed in an open transmission line connected with free space in such a way that the junctions interact with each other electrodynamically through their quasistatic fields and radiation fields. This line is shown schematically in Fig. 1. In contrast to [11, 12], where the transmission line was modeled merely by finite impedances over a period, we regard here the periodic line as a distributed object, where the impedance of the elementary cell depends explicitly on the length and design features of the cell, such as the presence of inhomogeneities, inductive short-circuits, and lateral stubs acting as antennas.
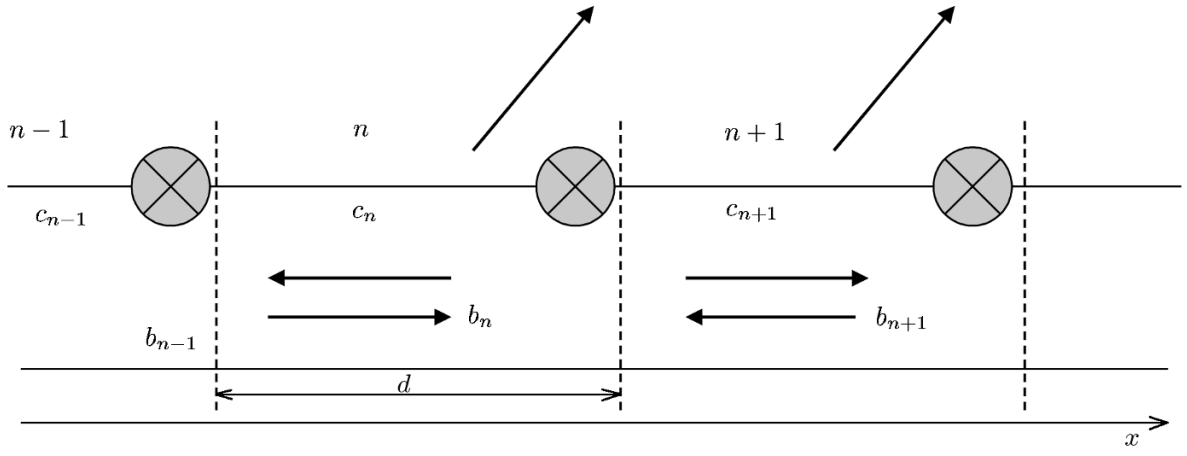
Fig. 1. Josephson junctions (shown by crosses) placed in a homogeneous line and forming a periodic structure. The arrows shows schematically the waves traveling in the line and radiating to free space. The dashed lines separating the neighboring periods mark the points of joining the current and the voltage in the line.

The equations for the complex amplitudes of the currents and voltages on the nth line period at a fixed frequency ω are expressed in terms of the amplitudes of the waves traveling to the right and to the left, and have the form

$$I_n = b_n \exp(ikx) + c_n \exp(-ikx), \qquad U_n = z_{\rm w}[b_n \exp(ikx) - c_n \exp(-ikx)] + U_{n,\rm J}. \qquad (1)$$

Here, I_n and U_n are the amplitudes of the current and voltage in the line, respectively, b_n and c_n are the amplitudes of the waves traveling to the left and to the right, respectively, $z_{\rm w}$ is the wave impedance of the line, $U_{n,\rm J}$ is the complex amplitude of the voltage across the Josephson junction, and the wave number is determined by the relation $k = (\omega + i\nu)/v$, where ω is the frequency, v is the velocity of wave propagation in the line, and the imaginary part of the wave number, which is determined by the parameter ν, simulates the loss for dissipation in the line and radiation to free space. The relation between the temporal and spectral representations (the functions $f(t)$ and $f(\omega)$, respectively) is determined in the standard manner:

$$f(\omega) = \int\limits_{-\infty}^{+\infty} f(t) \exp(i\omega t)\, {\rm d}t, \qquad f(t) = \int\limits_{-\infty}^{+\infty} f(\omega) \exp(-i\omega t)\, {\rm d}\omega/(2\pi), \qquad {\rm Im}\,\omega > 0.$$

The Josephson junctions included in the line will be regarded as lumped and described using a simple resistive shunt model, which is applicable at relatively low frequencies [11]. The equations of this model in the time representation have a simple form,

$$\frac{\Phi_0 C}{2\pi} \frac{\partial^2 \varphi_n}{\partial t^2} + \frac{\Phi_0}{2\pi R} \frac{\partial \varphi_n}{\partial t} + I_{\rm c} \sin \varphi_n = I_n, \qquad (2)$$

where φ_n is the Josephson phase difference of phases at the nth junction, $\Phi_0 = \pi\hbar/e = 2 \cdot 10^{-15}$ V·s is the flux quantum, C, R, $I_{\rm c}$ are the capacitance, resistance, and critical current of individual junctions, respectively, and $I_n(t)$ is the current through the nth contact, which includes the dc bias current and the ac current in the line. The voltage at the contact is determined by the Josephson relation

$$U_n(t) = \frac{\Phi_0}{2\pi} \frac{\partial \varphi}{\partial t},$$

where $2\pi/\Phi_0 = 0.486$ THz/mV. For the sake of simplicity, we will assume that the parameters of all Josephson junctions are identical. It is convenient to pass over to the dimensionless variables, adopting $I_{\rm c}$

as a unit of current, RI_c as a unit of voltage, and $\Omega^{-1} = 2\pi RI_c/\Phi_0$ as a unit of time. In these variables, Eq. (2) takes the form

$$\beta\ddot{\varphi}_n + \dot{\varphi}_n + \sin\varphi_n = I_n, \tag{3}$$

where the dots denote the time derivatives and β is the McCumber parameter determined by the relationship $\beta = \Omega RC$. In these variables, the voltage is $U_n = \dot{\varphi}_n$, and all impedances are measured in junction's resistances. The solution of the equations for the Josephson junctions will be found using the method of separation of fast and slow variables [11]. We will seek solutions in the form $\varphi_n = \omega_J t + \theta_n + \psi_n$, where the quantity ψ_n describes small high-frequency oscillations of the phase, θ_n is not a small, but slow phase variable, and ω_J is the frequency of the Josephson oscillations. Substituting these formulas into Eq. (2) for the Josephson phases, we obtain an equation for the unperturbed Josephson frequency $\omega_J = I$, where I is the bias current being common for all the contacts, the equation

$$\beta\ddot{\psi}_n + \dot{\psi}_n = I_n - \sin(\omega_J t + \theta_n) \tag{4}$$

for the high-frequency components, and the equations

$$\beta\ddot{\theta}_n + \dot{\theta}_n + \overline{\psi_n \cos(\omega_J t + \theta_n)} = 0, \tag{5}$$

for the slow phases, where the overbar denotes time averaging. Equation (4) is conveniently rewritten in complex form by introducing the complex amplitude Ψ such that $\psi = \mathrm{Re}[\Psi \exp(-i\omega_J t)]$. Then, Eqs. (4) and (1) for the complex amplitudes of the Josephson phases and the traveling waves in the line, respectively, take the form

$$b_n \exp(ik_J d) + c_n \exp-(ik_J d) = b_{n+1} + c_{n+1},$$

$$b_n \exp(ik_J d) - c_n \exp-(ik_J d) - \frac{i\omega_J \Psi_n}{z_w} = b_{n+1} - c_{n+1},$$

$$-(\beta\omega_J^2 + i\omega_J)\Psi_n = -i\chi_n + [b_n \exp(ik_J d) + c_n \exp(ik_J d)], \tag{6}$$

where we introduced the notation $\chi_n = \exp(-i\theta_n)$, d is the length of the elementary cell of the line (see Fig. 1), and k_J is the wave number corresponding to the frequency of the Josephson oscillations. Equation (5) for the slow motions is rewritten in the form

$$\beta\ddot{\theta}_n + \dot{\theta}_n + \frac{1}{2}\mathrm{Re}(\Psi_n \chi_n^*) = 0, \tag{7}$$

where the asterisk denotes complex conjugation. Equation (4) for high-frequency components of the Josephson phase and Eqs. (1) for the currents and voltages in the line are linear. They can be solved using the Fourier transform technique. The transforms will be determined either for a system with periodic boundary condition or for the infinite system as

$$A(q) = \sum_{n=0}^{N-1} A_n \exp(-iqn), \qquad A(q) = \sum_{n=-\infty}^{+\infty} A_n \exp(-iqn),$$

with the corresponding inversion formulas. For the periodic and infinite systems, we will have, respectively,

$$A_n = \frac{1}{N}\sum_{m=0}^{N-1} A\left(q = \frac{2\pi m}{N}\right)\exp\left(i\frac{2\pi m}{N}n\right),$$

$$A_n = \int_{-\pi}^{\pi} A(q)\exp(iqn)\frac{\mathrm{d}q}{2\pi},$$

where the function $A(q)$ is understood as either of the functions $b(q)$, $c(q)$, $\psi(q)$, and $\chi(q)$ which are the Fourier transforms of b_n, c_n, ψ_n, and χ_n (i.e., A_n), respectively, and N is the number of Josephson junctions. The equations for the high-frequency components are solved easily in terms of the Fourier harmonics. For the amplitudes of the waves traveling to the left and to the right, we have, respectively,

$$b = \frac{i\omega_{\mathrm{J}}\psi}{2z_w} \frac{1}{\exp(ik_{\mathrm{J}}d - iq) - 1}, \qquad c = \frac{i\omega_{\mathrm{J}}\psi}{2z_w} \frac{1}{\exp(-ik_{\mathrm{J}}d - iq) - 1}, \tag{8}$$

and the equation for the high-frequency phase perturbation has the form

$$-(\beta\omega_{\mathrm{J}}^2 + i\omega_{\mathrm{J}})\psi(q) = -i\chi + i\omega_{\mathrm{J}}\psi(q)Y(q,\omega_{\mathrm{J}}), \tag{9}$$

where $Y(q,\omega)$ is the Fourier transform of the admittance of the transmission line, which is determined by the relation

$$Y(q,\omega) = \frac{1}{2z_w} \frac{-i\sin(kd)}{\cos q - \cos(kd)}. \tag{10}$$

This formula is the Green's function, which determines the linear response of the unperturbed line without Josephson junctions. Vanishing of the denominator yields a dispersion relation for the eigenwaves in the transmission line, i.e., $\cos(kd) = \cos q$. In the scheme of expanded zones, it yields just a linear dispersion ($kd = q$) of a smooth two-wire line. Finally, for the Fourier amplitude of the high-frequency Josephson phase, we have $\psi(q) = G(q)\chi(q)$, where the Green's function $G(q)$ is determined by the formula

$$G(q) = \frac{i}{\beta\omega_{\mathrm{J}}^2 + i\omega_{\mathrm{J}}[1 + Y(q,\omega_{\mathrm{J}})]}. \tag{11}$$

Getting back to the coordinate representation, we find the solution for high-frequency amplitudes

$$\Psi_n = \sum_m G(n - m, \omega_{\mathrm{J}})\exp(-i\theta_m), \tag{12}$$

where the Green's function in the coordinate representation is determined either as the integral along the Brillouin zone for the infinite system, i.e.,

$$G(n,\omega_{\mathrm{J}}) = \int_{-\pi}^{\pi} G(q,\omega_{\mathrm{J}})\exp(iqn)\frac{\mathrm{d}q}{2\pi}, \tag{13}$$

or as the sum of the permitted values of the momentum $q_l = 2\pi l/N$ for the periodic line:

$$G(n) = \frac{1}{N}\sum_{l=0}^{N-1} G(q_l)\exp(iq_l n). \tag{14}$$

Now, having an explicit formula for high-frequency amplitudes, we can write dynamic equations for the slow phases of the Josephson junctions:

$$\beta\ddot{\theta}_n + \dot{\theta}_n + \frac{1}{2}\mathrm{Re}\left[\exp(i\theta_n)\sum_m G(n - m, \omega_{\mathrm{J}})\exp(-i\xi_m)\right] = 0. \tag{15}$$

This complex system of nonlinear dynamic equations for slow Josephson phases was deduced in [11, 12], where some of its particular solutions were also considered. The features of the electrodynamic environment is described by the function $Y(q,\omega)$ and the function $G(q,\omega)$, which is determined by the former junction. Therefore, for an arbitrary, spatially periodic linear transmission line, the dynamics equations for the

Josephson junctions have the form

$$\beta\ddot{\varphi}_n + \dot{\varphi}_n + \sin\varphi_n = I - \sum_m \hat{Y}_{n-m}\dot{\varphi}_m, \tag{16}$$

where $\hat{Y}_{n-m}$ is the admittance matrix, which determines the current $I_n(t) = -\sum_m \hat{Y}_{n-m}U_m(t)$ through the junction and, thus, describes the electrodynamic influence of the mth junction on the nth one. If the system is not spatially periodic, then the admittance matrix is merely a general matrix rather than a function of the difference $n - m$. Each matrix element is the operator $\hat{Y}$ acting on the time function $f(t)$ as

$$\hat{Y}f(t) = \int_{-\infty}^{t} Y(t - t')f(t')\,dt', \tag{17}$$

and determines the delay interaction between the Josephson elements of the system. Thus, in the general case, the Josephson dynamics is described by a system of complex integro-differential equations. In the coordinate representation, the admittance $Y(q)$ in Eq. (10) corresponds to the admittance in real space, which is determined by the formula

$$Y_n = -\frac{1}{2z_{\mathrm{w}}}\exp(ikd\,|n|), \tag{18}$$

which has a simple physical meaning: it determines the coupling of the junctions via the wave traveling in the line. The scale of localization of the Green's function is found from the imaginary part of the wave number, which is determined by the loss in the line due to radiation to free space and the true Joule loss.

In the case of an arbitrary line, the transmission-line admittance is a complicated function of the frequency and the wave number. Moreover, in the general case of open systems, as is well known in the antenna theory [13], the current distribution in the antenna depends on the distribution of electromotive forces on it, which means that the matrices of mutual admittances are functionals of the phase distribution of oscillations of the Josephson junctions. To study the dynamics of such systems, direct solution of the Maxwell equations along with the dynamic equations for the Josephson junctions is required. This is the subject of Sec. 4 of this paper. In the next section, we will consider the possibility of simple solutions of the traveling-wave type in system (15) for various types of the kernel $G(n - m)$.

3. TRAVELING-WAVE REGIME AND ITS STABILITY

Consider system of Eq. (15). Due to the fact that the system is periodic and the Green's function depends only on the difference $m-n$, it has a solution in the traveling-wave form for the phases $\theta_n = \theta_0 - q_1 n$. Substituting this solution into Eq. (15), we find the equation for the phase of the zeroth (and, consequently, any other) junction:

$$\beta\ddot{\theta}_0 + \dot{\theta}_0 + \frac{1}{2}\mathrm{re}\left[\exp(i\theta_0 - iq_1 n)\sum_m G(n - m, \omega_{\mathrm{J}})\exp(-i\theta_0 + iq_1 m)\right] = 0. \tag{19}$$

This equation determines the stationary-state onset and the correction for the current–voltage characteristics of the Josephson junctions. The sum in Eq. (19) can be evaluated. Then, this equation takes the form

$$\beta\ddot{\theta}_0 + \dot{\theta}_0 + \frac{1}{2}\mathrm{Re}G(q_1) = 0, \tag{20}$$

where $G(q_1) = \sum_m G(n - m)\exp[-iq_1(n - m)] = \sum_m G(m)\exp(-iq_1 m)$. Hence it follows that in the steady-state regime, where $\ddot{\theta}_0 = 0$, the correction to the Josephson frequency and, thus, to the current–voltage characteristic is determined by the relation $\delta\omega_{\mathrm{J}} = -\mathrm{Re}G(q_1, \omega_{\mathrm{J}} = I)/2$. Note at once that since only $\dot{\theta}_0$ appears in the equation, the solution for the phase is determined with accuracy up to an arbitrary constant.

Knowing the phases of junction oscillations, we can determine the wave amplitudes at each period, find the distribution of the current in the line, and calculate the radiation to free space. Taking into account that the equality

$$\chi(q) = \exp(-i\theta_0) \sum_{n=0}^{N-1} \exp[i(q_1 - q)n] = \exp(-i\theta_0) N \, \delta_{q_1,q},$$

where $\delta_{q_1,q}$ is the Kronecker delta, is fulfilled in the traveling-wave regime, calculating the amplitudes of the waves travelling to the right and to the left, and finding the current on each period, we arrive at the formula

$$I_n(x) = \frac{i\omega_J G(q_1) \exp(-i\theta_0 + iq_1 n)}{2z_w} \left\{ \frac{\exp[ik_J(x-nd)]}{\exp(ik_Jd - iq_1) - 1} + \frac{\exp[-ik_J(x-nd)]}{\exp(-ik_Jd - iq_1) - 1} \right\}. \tag{21}$$

It follows from here that the Josephson line under consideration is a one-dimensional array of identical dipoles with length d and identical, but phase-shifted current distributions. Assuming that the transmission line is a single-wire line, we expand the current distribution corresponding to Eq. (21) into a Fourier series in terms of the harmonics with the spatial frequencies $k_m = 2\pi m/d$ and find that

$$I(k_m) = \frac{i\omega_J N G(q_1) \exp(-i\theta_0)}{2z_w} \left\{ \frac{\exp[i(k_J - k_m)d] - 1}{\exp(ik_Jd - iq_1) - 1} + \frac{\exp[-(k_J + k_m)d] - 1}{\exp(-ik_Jd - iq_1) - 1} \right\} \delta_{q_1,k_md}. \tag{22}$$

From here, it is seen that such an antenna array radiates coherently in the direction of the generatrix of a cone with the opening angle $\alpha = \arcsin[c_{light} q_1/(\omega_J d)]$, where c_{light} is the speed of light in free space, since the amplitude of the current harmonic is proportional to N. On the other hand, if the wave number q_1 is sufficiently large, such that $\alpha > 1$, then the radiated wave is bound to the wire, and the radiation occurs only from the ends of the system. In our solution, the wave number of the traveling wave is a free parameter. Therefore, the question of which of the solutions is realized, or whether this regime can be realized at all, requires studying a nonstationary nonlinear problem with certain initial conditions.

However, the precondition for realization of the traveling-wave regime under consideration is the regime stability with respect to small perturbations, which will be studied now.

Let us put $\theta_n = \theta_0 - q_1 n + \delta\theta_n$ and linearize Eq. (15) assuming that $\delta\theta_n \ll 1$. As a result, we obtain N real linear equations for slow variations in the phase differences:

$$\beta \, \delta\ddot{\theta}_n + \delta\dot{\theta}_n + \sum_m K(n-m)\,(\delta\theta_n - \delta\theta_m) = 0, \tag{23}$$

where the kernel is determined by the formula $K(n-m) = 0.5\,\mathrm{Re}\, iG(n-m) \exp[-iq_1(n-m)]$. Searching for a solution in the form $\delta\theta_n = \delta\theta(q) \exp(iqn - i\omega t)$, we arrive at the dispersion relation

$$-(\beta\omega^2 + i\omega) + Q(q) = 0, \tag{24}$$

where $Q(q) = K(0) - K(q)$, while the Fourier transform of the kernel K is expressed in terms of a Fourier transform of the kernel G by the following relationships:

$$K(q) = \frac{i}{4}[G(q+q_1) - G^*(-q_1-q)], \qquad K(0) = \frac{i}{4}[G(q_1) - G^*(-q_1)]. \tag{25}$$

Dispersion relation (24) determines the frequency $\omega = \omega(q; q_1, \omega_J)$ as a function of the parameters q_1 and ω_J of the initial nonlinear solution. It is important to pay attention to the existence of the zero eigenvalue at $q = 0$, which is related to the symmetry with respect to the global shift of all phases. Thus, finally, we have the dispersion relation $\beta\omega^2 + i\omega = Q$, where

$$Q(q, q_1) = \frac{i}{4}[G(q_1) - G^*(-q_1)] - \frac{i}{4}[G(q+q_1) - G^*(-q_1-q)]. \tag{26}$$
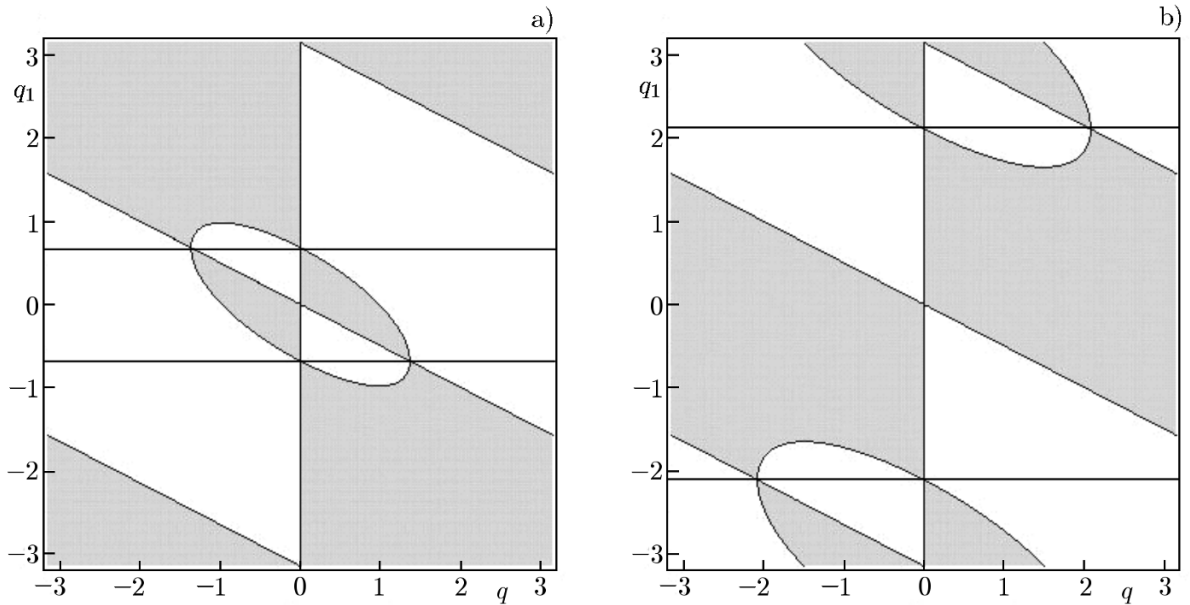
Fig. 2. Regions of stability and instability of the traveling-wave regime on the plane (q, q_1) for $\omega_J d/v = 0.3\pi/2$ (*a*) and $\omega_J d/v = 1.3\pi/2$ (*b*). The wave impedance of the line is equal to $z_w = 4$ and the loss, to $\nu/v = 0.01$. The horizontal lines mark the wave numbers of the stable solutions of the traveling-wave type. It is seen that as the parameter $\omega_J d/v$ increases, the wave number of the stable traveling wave also increases.

It is easily seen that the stability region determined by the condition $\text{Im}\,\omega < 0$ corresponds to the inner zone of the parabolic curve $\text{Re}\,Q > \beta(\text{Im}\,Q)^2$. However, in the special case considered here, the function G is an even function of the wave vector $(G(q) = G(-q))$. Therefore, the function $Q(q)$ is real, and the stability condition is formulated simply as $Q > 0$.

To analyze the system stability, we plot a series of zero isolines on the plane (q, q_1), which are determined by the equation $Q(q, q_1) = 0$, for different values of the other parameters. Typical patterns of these isolines for two values of $\omega_J d/v$ are shown in Fig. 2. The white area corresponds to the condition $Q > 0$ and stability of the traveling-wave regime. If there exists the straight line $q_1 = q_s$, which belongs entirely to the white region, then the corresponding traveling-wave regime is stable. Note the evident symmetry with respect to the replacements $q \to -q$ and $q_1 \to -q_1$, which leaves the coefficient Q to be invariant. This symmetry manifests itself in the symmetry of the pattern with respect to a turn by the angle π around the origin of the coordinates.

The parameter $Q(q, q_1 = q_s)$ is always positive, except for two points, $q = 0$ and $q = q_{\min} = -2q_1$, which indicates that the stability of the nonlinear solution is neutral, or marginal with respect to the excitation of modes with these wave numbers. The origin of zero values of the function $Q(q)$ is related to the degeneracy of the nonlinear solution. The point $q = 0$ is related to the symmetry of the nonlinear solution with respect to translations and corresponds to infinitesimally small perturbations in the form of a shift of the nonlinear solution as a whole $(\theta_0 \to \theta_0 + \delta\theta_0)$. The second point, $q = q_{\min} = -2q_1$, is related to the existence of a nonlinear solution differing from the consideret one in that the propagation direction changes, i.e., $q_1 \to -q_1$. The linear perturbations with the wave vector $q = q_{\min} = -2q_1$ correspond to the possibility of excitation of this mode. Degeneracy of the nonlinear solutions is eliminated in finite systems due to violation of translational invariance, which prohibits a mode with $q = 0$. One can eliminate the degeneracy $q = \pm q_1$ by imposing suitable boundary conditions at different ends of the system.

As the dimensionless elementary period $\tilde{z} = \omega_J d/v$ of the line increases, the plot of the function $q_1(\tilde{z})$ forms a continuous curve, which is shown qualitatively in Fig. 3.

It is important to note that the purely in-phase ($q_1 = 0$) and purely anti-phase ($q_1 = \pi$) regimes do not have finite stability zones, except for the isolated points $z = 0$ and π, which apparently contradicts
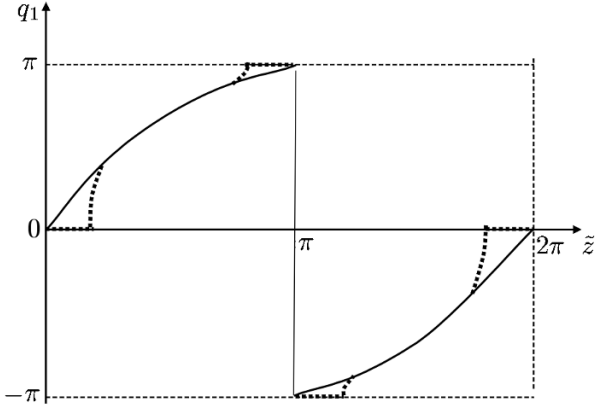
Fig. 3. Dependence of the wave number q_1 of the traveling wave in the stable regime on the elementary period $\tilde{z} = \omega_J d / v$. The dotted lines show the distortion of the dependence $q_1(\tilde{z})$ and appearance of purely in-phase and purely anti-phase regimes due to inclusion of inductive short-circuits, which make the transmission line periodic, with finite forbidden bands, even in the absence of the Josephson junctions.

the common concepts formulated in, e.g., [11]. This apparent contradiction is explained by the fact that we consider the transmission line as a distributed object, in which wave reflection is determined by the presence of the Josephson junctions only. In other words, in the absence of Josephson junctions, there are no singled-out frequencies in the eigenmode spectrum of the transmission line. The dispersion relation corresponding to the zero denominator in Eq. (10) corresponds to the absence of forbidden bands. As a result, the phases of reflected waves in such a line are determined self-consistently by the phase of the Josephson oscillations, which leads to a continuous dependence of the wave number of the traveling-wave nonlinear solution on the dimensionless period $\tilde{z}$.

In [11, 12], the line period was simulated by means of lumped elements. We will show that inclusion of such elements as, e.g., inductive short-circuits, in the line leads to possible stabilization of both in-phase ($q_1 = 0$) and anti-phase ($q_1 = \pi$) regimes. Consider a line with inductive short-circuits located slightly on the left of the joining points shown in Fig. 1 by dashed lines. In this case, the equations for the wave traveling in the line and the high-frequency phase oscillations take the form

$$b_n \exp(ik_J d) + c_n \exp(-ik_J d) = \frac{z_w}{-i\omega_J L}(b_{n+1} - c_{n+1}) + b_{n+1} + c_{n+1},$$

$$b_n \exp(ik_J d) - c_n \exp(-ik_J d) - \frac{i\omega_J \Psi_n}{z_w} = (b_{n+1} - c_{n+1}),$$

$$-(\beta\omega_J^2 + i\omega_J)\Psi_n = -i\chi_n + [b_n \exp(ik_J d) + c_n \exp(-ik_J d)].$$

Here, in contrast to Eq. (6), additional terms have appeared, which allow for the contribution of the inductive short-circuit, and L is the self-inductance of the short-circuit. Introduction of the inductive short-circuits makes the line periodic already in the absence of the Josephson junctions. Such additional terms do not change the general view of the dynamic equations, and only lead to a change in the form of the admittance. Instead of Eq. (10), we have a slightly modified formula

$$Y = \frac{-i\sin(k_J d) - \dfrac{z_w}{i\omega_J L}\cos(k_J d)}{2z_w\left[\cos q - \cos(k_J d) - \dfrac{z_w}{2\omega_j L}\sin(k_J d)\right]}, \tag{27}$$

which transforms to that presented earlier for a sufficiently high inductance ($z_w/(\omega_J L) \to 0$). Equating the denominator to zero, we find the dispersion relation

$$\cos q = \cos(k_J d) + \frac{z_w}{2\omega_J L}\sin(k_J d),$$

which determines the wave spectrum. In the case of a finite inductance, this is a spectrum with finite widths of the forbidden bands, which should influence the dynamics of the system under consideration. The plots which illustrate the influence of inductive short-circuits and the appearance of stable, purely in-phase and anti-phase regimes are shown in Fig. 4. Figure 4a corresponds to the stable, purely in-phase regime ($q_1 = 0$), which is realized in the neighborhoods of the values of the period $\tilde{z} = 2\pi n$, which are
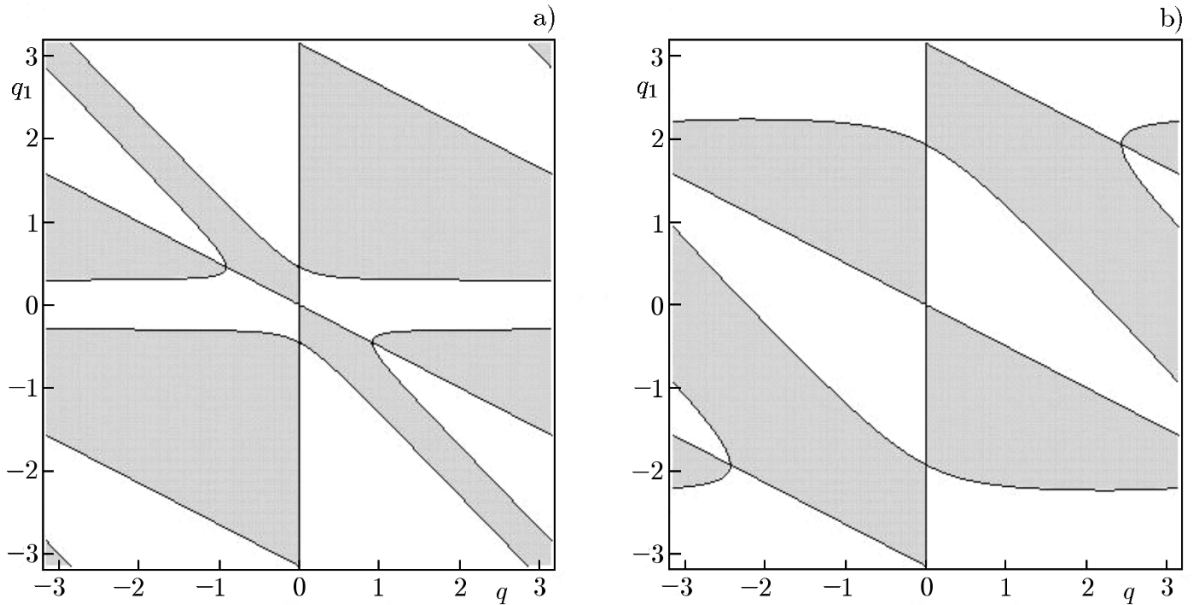
Fig. 4. Regions of stability and instability of the in-phase ($q_1 = 0$) and anti-phase ($q_1 = \pi$) regimes for a finite short-circuit inductance $L = 10$ for two values of the parameter $\tilde{z} = \omega_J d/v$: $\tilde{z} = 0.2\pi/2$ (*a*), which corresponds to the stability of the in-phase regime, and $\tilde{z} = 1.95\pi/2$ (*b*), which corresponds to the stability of the anti-phase regime. The wave impedance of the line is equal to $z_w = 4$ and the loss, to $\nu/v = 0.01$. The in-phase and anti-phase regimes become stable near the center and the edge of the Brillouin zone, respectively.

multiple of the wavelength in the line. Figure 4*b* corresponds to the stability of the purely anti-phase regime taking place in the neighborhoods of the values of the line period $\tilde{z} = \pi(2n + 1)$, which are multiple of an odd number of half-waves. The width of the regions in which the purely in-phase and anti-phase regimes exist is determined by the ratio of the inductance and the wave impedance of the line. One should pay attention to a significant difference in the stability patterns of the purely in-phase and anti-phase regimes from the patterns corresponding to the traveling waves shown in Fig. 2. For traveling waves, there are two neutrally stable modes, $q = 0$ and $q = q_{\min} = -2q_1$, and for pure regimes, only one mode with $q = 0$ is left. The appearance of purely in-phase and anti-phase stable regimes is shown in Fig. 3 by dotted lines. One can see that the pure regimes correspond to the center and the edge of the Brillouin zone. It becomes fairly clear that the appearance of the pure in-phase and anti-phase regimes occurs due to the zonal character of the spectrum of line eigenwaves in the absence of the Josephson junctions. These pure states are realized near the center and the edge of the Brillouin zone, whereas the traveling-wave regime takes place in the depth of the zone.

We now discuss the possibilities of the traveling-wave regime in a finite system with boundary conditions at the ends. The boundary impedances should specially be chosen in such a way as to ensure that the amplitude and phase relationships between the amplitudes of the counterpropagating waves in the end sections of the periodic lines are close to the relationships in the traveling wave in an infinite system. To ensure smooth frequency tuning, one should vary the boundary conditions smoothly and consistently, which can be achieved by using electrically controlled elements based on semiconductors or superconductors. Evidently, this rather difficult problem can be solved only in certain frequency ranges.

In order to describe the actual systems with Josephson junctions, such as inhomogeneous transmission lines, power circuits, lumped elements, microantennas, matching elements, etc., we have developed a software code for direct numerical simulation, which calculates self-consistently the dynamics of the electromagnetic field and the Josephson junctions.

4. SIMULATION OF JOSEPHSON ANTENNAS

We have seen in the previous sections that in order to describe the dynamics of the Josephson junctions and merely to formulate the dynamic equations in the form of Eq. (16), one should know the admittance matrix, which determines the coupling among the contacts. This matrix is determined by the electrodynamic environment, and each matrix element is a complex function of the frequency, which corresponds (in the time representation) to complex nonlocal integral operator (17). If the Josephson system has small sizes (compared with the wavelength), then the matrix elements of the admittances are rational frequency functions or, in other words, are determined by mutual capacitances, inductances, and resistances. In the time representation, this corresponds to that the admittance operators can be represented by finite-order time-differential operators, and the entire dynamic system of type (16) is a system of differential equations. If the size of the system is comparable with or exceeds the wavelength, then the delay effects are important, and Eq. (16) yields a system of nonlinear integro-differential equations. However, the situation is even more complicated: in a certain sense, the admittance matrix in the system of type (16) is merely undefined. The thing is that in the general case of open system (which is a well-known fact in the antenna theory [13]), the current distribution in the antenna depends on the distribution of electromotive forces along the antenna. In turn, this means that the mutual-admittance matrices are functionals of the distribution of oscillation phases of the Josephson junctions. In order to gain insight into these complicated issues, we performed numerical simulation based on direct numerical solution of the Maxwell equations together with the dynamic equations of the Josephson junctions.
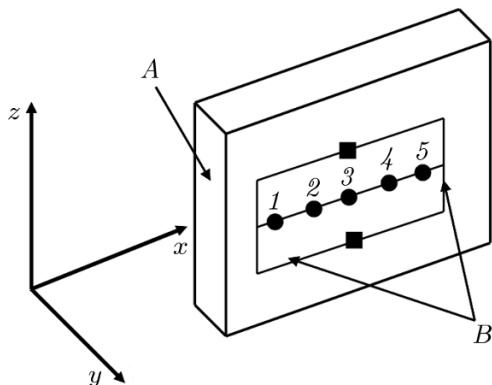

Fig. 5. Scheme of the simplest Josephson antenna in the form of a straight wire with included Josephson junctions *1–5* located on the dielectric plate *A*. The circles show and the squares show the power supply batteries and the Josephson contacts, respectively. The perfect conductors are denoted by the symbol *B*. The used systems of coordinates is also shown.

To study the nonlinear dynamics of the active Josephson antennas, we have developed a software code based on solving the Maxwell equations by the FDTD method and on the self-consistent solution of the nonlinear equations describing the dynamics of the Josephson junctions. It turns out to be impossible to use standard electrodynamic-simulation software suites, such as, e.g., "CST Microwave Studio" [14], to solve the problem under consideration because of the necessity to calculate self-consistently the dynamics of the Josephson junctions.

An example chosen for the calculations is a Josephson system similar to the single-wire traveling-wave antenna called the Beverage antenna [10]. The simulated Josephson system is a system of thin perfect conductors, lumped linear elements, such as capacitors, inductances, resistors, and sources of constant electromotive forces, and nonlinear active elements (Josephson junctions). These elements are located on the surface of a dielectric plate and interact via the electromagnetic field in the surrounding space. An example of such a system representing an antenna in the form of a straight wire with five Josephson junctions included in it and power circuits fed by two batteries with high internal resistances, which are located on the flat surface of a dielectric substrate, is shown in Fig. 5.

For numerical simulation of the field dynamics, the Maxwell equations were represented by the finite-difference scheme proposed for the first time in [15]. This scheme is obtained by writing equations for the field components on a grid with an elementary cell in the form of a parallelepiped. The components E_x, E_y, and E_z of the electric field are assumed to be specified at the corresponding edges of the elementary cells of the grid, while the components B_x, B_y, and B_z, at the centers of the faces. The differential vector operations of divergence and curl are represented as fluxes through the faces and circulations along the edges

of elementary circles, respectively. To perform the time step, we use the explicit Euler method (FDTD). Currently, it is used for a wide range of problems, from calculation of microantennas to simulation of wave propagation in the urban environment [16].

The modeled Josephson antenna consists of perfect conductors, which are thin compared with all characteristic scales, so that the transverse distribution of the current in them can be regarded as homogeneous. These wires, as well as the components of the electric field, are assumed to be concentrated on the cell edges. The boundary condition at a perfect conductor, which corresponds to the equality of the tangential component of the electric field to zero, is simulated by the equality of the field on the corresponding edge to zero. The Josephson junction is simulated by the chosen cell edge, at which the field dynamics is determined by the Josephson contact equations rather than a free Maxwell equation. The dynamics of the junction is described by a system of ordinary differential equations for the phase difference φ and the corresponding component of the electric field, e.g., E_x, on the cell edge, which contains a junction:

$$\frac{\partial \varphi}{\partial t} = \frac{2\pi}{\Phi_0} E_x d, \qquad dC\frac{\partial E_x}{\partial t} + \frac{dE_x}{R} + I_c \sin\varphi = I, \qquad I = S\left(\mathrm{rot}\,\mathbf{B} - \varepsilon_0 \frac{\partial \mathbf{E}}{\partial t}\right)_x. \tag{28}$$

In this equation, Φ_0 is the quantum of the magnetic-field flux, C and R are the capacitances and the intrinsic resistance of the junction, I_c is the critical current of the junction, d and S are the length of the edge and the area of the chosen cell of the grid, respectively, and ε_0 is the electric constant. In the software, this system is solved by the semi-implicit Crank–Nicolson method [17]. Note that any lumped element can be modeled in a similar way: one should only replace dynamic equation (28) by the relation of the current and voltage of the corresponding element. The power supply is also simulated by the singled-out edge of the grid, on which the dynamics of the electric field is described by the equations

$$IR_b = dE_x - \mathcal{E}, \qquad I = S\left(\mathrm{rot}\,\mathbf{B} - \varepsilon_0 \frac{\partial \mathbf{E}}{\partial t}\right)_x. \tag{29}$$

Here, $\mathcal{E}$ is the electromotive force of the source, R_b is its internal resistance, and the b subscript means the source number. This equation is also solved using the implicit scheme.

The entire simulated circuit including the wires, Josephson junctions, power supplies, and the dielectric substrate, is surrounded with a certain free space, which is bounded on the outside by a layer of a special artificial medium simulating reflectionless boundary conditions. Many different types of such conditions are described in the literature [16]. Here, we use boundary conditions in the form of a perfectly matched layer (PML) [18, 19]. The layer of the artificial medium is chosen to be sufficiently thick, so as to achieve a negligibly low reflection. On the external surface of this reflectionless layer, zero conditions are specified for the tangential components of the electric field. Thus, a closed mathematical model is formulated to describe the dynamics of the Josephson circuit and the surrounding field. The 3D simulator code described here is the development of the two-dimensional model which we proposed earlier [20].

Setting the Josephson phases of the junctions and the electric and magnetic fields on the grid at the initial time allows us to start the calculations, which then go on continuously until the onset of the stationary regime in each junction. Then, after reaching the stationary-oscillation regime, we calculate the time average and Fourier amplitudes of the voltage and the currents I_b of the Josephson junctions. Knowledge of these values allows one to find the energy parameters such as, e.g., the power $\Sigma_b \mathcal{E}_b \bar{I}_b$ consumed by the microchip from the batteries, where the sum is taken over all power supply elements, or the power $\Sigma_m R_m^{-1}\overline{U_m^2} + \Sigma_b R_b \overline{I_b^2}$ dissipated in the resistances of the junctions and the internal resistances of the batteries. Here, R_m and U_m are the resistance of the mth Josephson junction and the voltage across it, respectively. The difference in the consumed and dissipated powers yields the total power emitted to free space. Along with the total powers, we can calculate the consumed and dissipated powers at fixed frequencies by using the Fourier transform with respect to time. For example, the power consumed by an individual junction is equal to $P_c = \mathrm{Re}(U_\omega I_\omega^*)/2$, the dissipated power is $P_d = \mathrm{Re}(R^{-1}U_\omega U_\omega^*)/2$, and their difference yields the work $P_s = \mathrm{Re}[I_c(\sin\varphi)_\omega U_\omega^*]/2$ of the supercurrent through each junction, which is spent for radiation to free space and dissipation in the
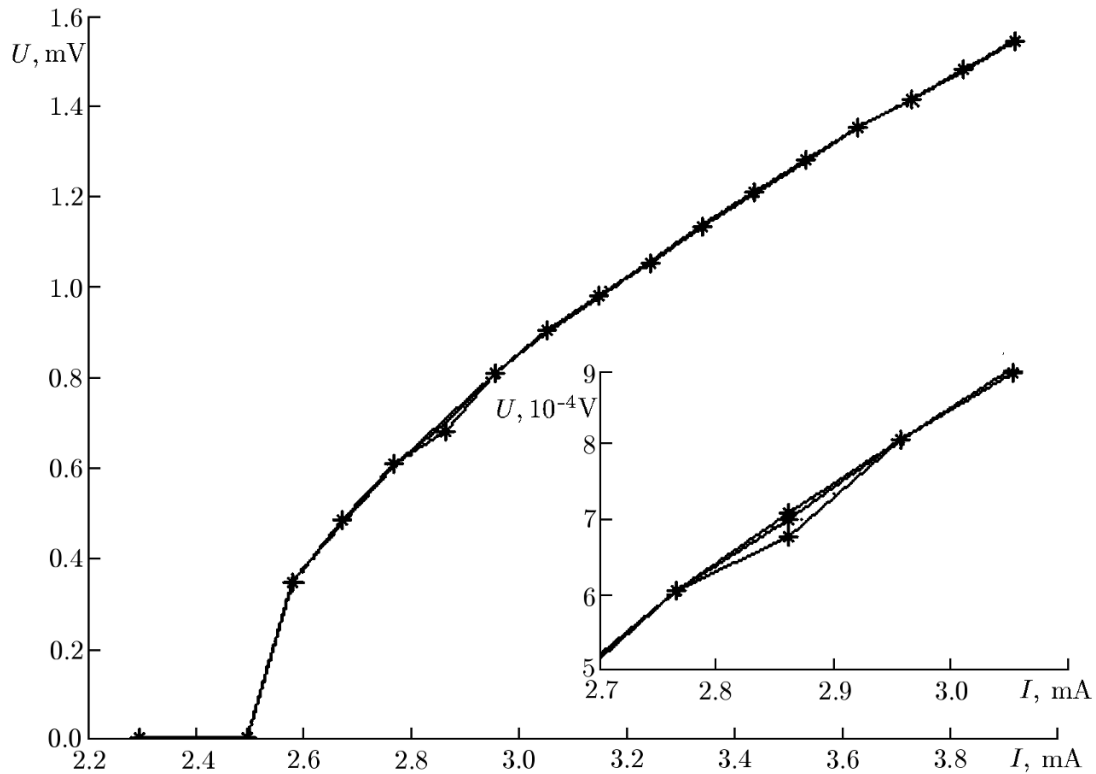
Fig. 6. Calculated current–voltage characteristics of the Josephson junctions which excite the antenna. The junctions are identical, and have the parameters $C = 100$ pF, $R = 0.5$ Ω, and $I_c = 2.5$ mA. One can discern the regions in which the current–voltage characteristics coincide, and the regions in which the curves differ noticeably. The inset shows one of the regions in which the junction parameters are different. One can see three curves, which correspond to junctions *1* and *5*, *2* and *4*, and *3* (see Fig. 5). The current–voltage characteristics of the junctions located symmetrically with respect to central contact *3* coincide. The coincidence of the current–voltage characteristics indicates that the oscillation frequencies are identical, whereas the absence of coincidence shows that there is no synchronization.

power supply elements. Here, I_ω and U_ω are the Fourier amplitudes of the current through and the voltage across the corresponding junction and $(\sin\varphi)_\omega$ is the Fourier transform of the function $\sin\varphi$. Slightly varying the power-supply voltage $\mathcal{E}_b$ using the values of the variables at a finite time instant as the initial ones for the new value of $\mathcal{E}_b$, and multiply repeating the calculations, one can obtain the dependence of all physical values on the power-supply voltage.

Figure 6 shows the calculated current–voltage characteristic of all five junctions. One can discern the regions in which the current–voltage characteristics coincide and the regions in which the curves are noticeably different. Coincidence of the current–voltage characteristics indicates that the oscillation frequencies are identical, whereas their difference indicates the absence of synchronism.

Figure 7 shows the total power $P_s = \text{Re}[\Sigma_m (U_{m\omega} I_{m\omega}^* - R^{-1} U_{m\omega} U_{m\omega}^*)/2]$ of the supercurrent as a function of the bias voltage $\mathcal{E}_b$. The quantities $U_{m\omega}$ and $I_{m\omega}$ are the Fourier amplitudes of the voltage across and the current through the mth junction, respectively, which are calculated at the harmonic of the Josephson frequency corresponding to the maximum amplitude $I_{1,\omega}$ of the ac current of the first junction. Less the minor power dissipated in the internal resistances of the batteries, which are assumed to be sufficiently great (200 Ω), this curve characterizes the power radiated to free space. It is seen that the simulated system is sufficiently narrow-band, and the radiation intensity varies significantly with frequency. Depending on the bias current, the regions with high radiation intensity alternate. The maximum radiation intensity was $P_{\text{rad}} \approx 2.4 \cdot 10^{-8}$ W for bias currents of about 3 mA, which corresponded to a rather good coefficient of
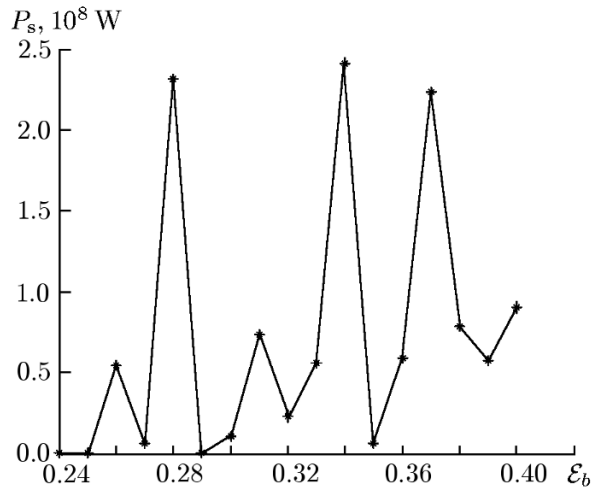
Fig. 7. Total power P_s of the supercurrent, which characterizes radiation to free space, as a function of the bias voltage. Great ruggedness of the curve on the plot is due to a strong dependence of the electrodynamic coupling parameters and the coupling conditions on the frequency.
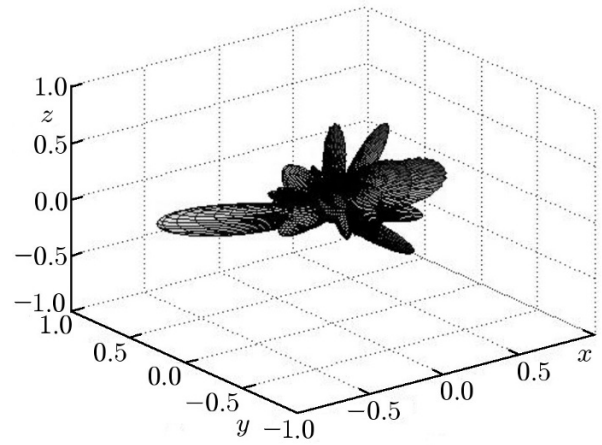

Fig. 8. Radiation pattern of the simulated Josephson antenna for a bias voltage of 0.34 V corresponding to the maximum power of the supercurrent shown in Fig. 7. A well-pronounced asymmetry of the radiation in the direction of the x axis is indicative of the traveling-wave regime. The multi-lobe character of the pattern is due to a large (compared with the radiation wavelength) size of the antenna.

battery-energy conversion to radiation, at a level of one percent.

To find the angular distribution of the radiation intensity at a fixed frequency, we used the standard method of the near-to-far field calculation [16]. This method was used in the following way. The entire simulation period for each bias voltage was divided into three intervals. At the first stage, we just waited for the onset of the stationary-oscillation regime. At the second stage, which followed the first one, the Fourier harmonics were calculated on the basis of the recorded realization of the current through the first junction, and the frequency at which the current harmonic was maximum was found. At the third simulation time interval, knowing the frequency ω, we calculated the Fourier harmonics of the tangential electric and magnetic fields at a certain surface shaped as a parallelepiped and determined the electric and magnetic surface currents $\mathbf{j}_e = [\mathbf{n} \times \mathbf{H}_\omega]$ and $\mathbf{j}_m = -[\mathbf{n} \times \mathbf{E}_\omega]$, respectively, where $\mathbf{n}$ is the outward directed normal to the surface. This surface enclosed the simulated circuit with the dielectric substrate and lied within the free-space domain, without reaching the boundary of the reflectionless layer. Then, based on the values of the complex amplitudes of the surface currents and the standard formulas, we calculated the far-zone fields, the Poynting vector, and the radiation patterns. Figure 8 shows an example of the radiation pattern, which was calculated for the bias voltage corresponding to the maximum power of the supercurrent. One can see that the radiation pattern is extended strongly along the x axis, which is aligned with the direction of the wire with the Josephson junctions. This indicates that the traveling-wave regime is realized.

Integration of the radiation pattern over all angles yields the total radiated power. For the pattern shown in Fig. 8, the total radiated power turns to be equal to $2.28 \cdot 10^{-8}$ W, which is slightly less than the value $2.41 \cdot 10^{-8}$ W evaluated from the work of the supercurrent (see Fig. 7).

5. CONCLUSIONS

We have considered the possibility to realize the traveling-wave regime in the multi-junction Josephson systems. For the simplest variants of the open Josephson lines, we have demonstrated that one can create an efficient Josephson oscillator of the terahertz and subterahertz frequency ranges on the basis of the traveling-

935

wave systems. The traveling wave in the line ensures identity of the electrodynamic conditions under which the junctions operate, whereas the energy leakage to radiation in the lateral direction prevents saturation of the nonlinearity of individual junctions with small dynamic ranges. We have developed a software code for direct numerical simulation of Josephson microchips, such as microantennas, lumped elements, and power circuits. Using this code, we have studied a model of the Josephson antenna, which is similar to the simplest single-wire antenna. The possibility to realize the traveling-wave regime has been demonstrated.

REFERENCES

1. B. D. Josephson, *Phys. Lett.*, **1**, 251 (1962).

2. T. Van Duzer and Ch. W. Turner, *Principles of Superconductive Devices and Circuits*, Prentice Hall, Upper Saddle River, NJ (1999).

3. M. Darula, T. Doderer, and S. Beuven, *Sci. Technol.*, **12**, R1 (1999).

4. P. Barbara, A. B. Cawthorne, S. V. Shitov, and C. J. Lobb, *Phys. Rev. Lett.*, **82**, 1963 (1999).

5. S. P. Benz and C. J. Burroughs, *Appl. Phys. Lett.*, **58**, 2162 (1991).

6. V. P. Koshelets, and S. V. Shitov, *Sci. Technol.*, **13**, R53 (2000).

7. L. Ozyuzer, A. E. Koshelev, C. Kurter, et al., *Science*, **318**, 1291 (2007).

8. U. Whelp, K. Kadowaki, and R. Kleiner, *Nature Photon.*, **7**, 702 (2013).

9. M. A. Galin, A. M. Klushin, V. V. Kurin, et al., *Sci. Technol.*, **28**, 055002 (2015).

10. C. A. Balanis, *Antenna Theory: Analysis and Design*, Wiley-Interscience, Hoboken, NJ (2005).

11. K. K. Likharev, *Introduction to the Dynamics of Josephson Junctions* [in Russian], Nauka, Moscow (1985).

12. A. K. Jain, K. K. Likharev, J. E. Lukens, and J. E. Sauvageau, *Phys. Rep.*, **109**, No. 6, 309 (1984).

13. M. A. Leontovich and M. L. Levin, *Zh. Tekh. Fiz.*, **14**, 481 (1944); M. A. Leontovich, *Teor. Fiz.*, 291 (1985).

14. http://www.cst.com/Content/Products/MWS/Overview.aspx

15. K. S. Yee, *IEEE Trans. Antennas Propagat.*, **AP-14**, 302 (1966).

16. A. Taflove and S. C. Hagness, *Computational Electrodynamics: The Finite-Difference Time-Domain Method*, Artech House, Norwood, Ma. (2005).

17. J. Crank and P. Nicolson, *Proc. Camb. Phil. Soc.*, **43**, No. 1, 50 (1947).

18. R. Korada, A. T. Umashankar, and B. Benjamin, *IEEE Trans. Antennas Propagat.*, **AP-35**, No. 11, 1248 (1987).

19. J. P. Berenger, *J. Comput. Phys.*, **127**, 363 (1996).

20. I. A. Shereshevskii, A. M. Klushin, V. V. Kurin, and N. K. Vdovicheva, in: *Proc. Int. Conf. "Days on Diffraction," St. Petersburg, May 26–30, 2014*, p. 198.